ON THE ACCURACY OF VISCOUS AIRFOIL COMPUTATIONS USING SOLUTION-ADAPTIVE UNSTRUCTURED GRIDS*

P.C. Walsh† and D.W. Zingg‡
University of Toronto, Institute for Aerospace studies
4925 Dufferin Street, Downsview, Ontario, M3H 5T6, Canada

Abstract

The purpose of this research is to investigate the improvement in the accuracy of viscous airfoil computations obtained through a solution-adaptive gridding technique for unstructured grids. The basic solver utilizes a finite-volume method together with a multigrid algorithm to solve the steady compressible Navier-Stokes equations. Adaptive node addition is implemented through calculation of an adaptive criterion based on normalized density and Mach number differences. A solution-dependent retriangulation scheme is used to restructure the adapted grid consistent with the local flow conditions. Examples for laminar and turbulent flows over airfoils provide quantitative estimates of the reduction in global error resulting from grid adaptation. Errors on the solution-adaptive grids are typically reduced by 30 to 50% compared to those obtained on an unadapted grid with an equivalent number of nodes.

Introduction

Accurate computations of viscous aerodynamic flows require very fine grids [1]. This leads to high memory requirements and long run times. One means of reducing these requirements is solution-adaptive gridding. For unsteady flows in which flow features requiring high spatial resolution are moving, solution-adaptive gridding is virtually indispensable. To a somewhat lesser degree, this is also true of steady flows when the location of such flow features is difficult to know before running the simulation. In addition to reducing the computing time and memory required for a simulation, solution-adaptive gridding should also reduce the user expertise required for an efficient simulation.

In computing aerodynamic flows, grid clustering is required near stagnation points, shock waves, and trailing edges, in boundary layers and wakes, and near regions where the geometry has high curvature. The state of the art in solution-adaptive grid techniques for aerodynamic applications is reviewed in Ref. [2]. For inviscid flows, good results are obtained using Cartesian grids [3], unstructured grids [4], and structured grids [5] . For turbulent flows at high Reynolds number, Cartesian grids are inappropriate [3], while redistribution of the nodes of a structured grid produces fairly modest improvements in accuracy [6]. Consequently, unstructured grids are best suited to solution adaptation for this flow regime.

Unstructured grids for computing two-dimensional high Reynolds number turbulent flows can consist of triangles [5] or arbitrary polygons. A combination of triangles and quadrilaterals is usually used in the latter case [7]. The use of quadrilaterals is generally more accurate in boundary layers. However, it increases the complexity of a solution-adaptive gridding technique.

Despite impressive progress, there are many issues in solution-adaptive gridding which need to be addressed. In particular, quantitative studies of the error reduction obtained using grid adaptation are useful in comparing strategies. For example, Warren et al. [8] showed that a popular grid adaptation criterion, the basic undivided difference, can produce extremely poor results. The results of Ref. [8] also clearly show that although the goal of grid adaptation is to minimize the error in the solution, the criterion for adaptation should be based on the error in the local approximation to the governing equations. Additional grid resolution is not necessarily needed in regions where the solution is inaccurate. This error can be caused by numerical errors incurred elsewhere, where the approximation

†Graduate Student

‡Associate Professor, Member AIAA.

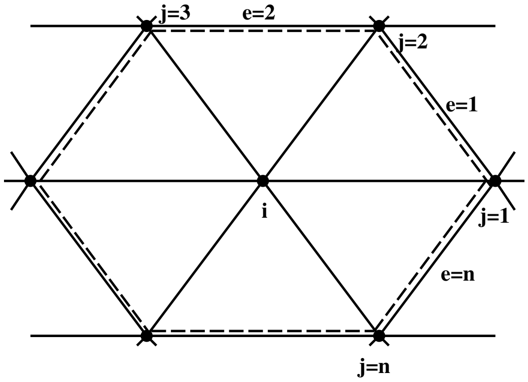

Figure 1: Typical Control Volume

is inaccurate.

The purpose of this paper is to present a detailed quantitative study of the error reduction resulting from a solution-adaptive gridding technique in the context of viscous flows over airfoils. The results provide an assessment of the technique used. Furthermore, the study enables our approach to be compared with other techniques and aids in the development of optimal strategies. In the next section the solution algorithm is described. It is based on the approach of Mavriplis and Jameson [9]. The adaptive gridding technique is then presented, including a solution-dependent retriangulation scheme. Finally, results are presented for laminar and turbulent flows over the NACA 0012 airfoil.

Numerical Algorithm

The equations describing the behavior of compressible viscous flow are the Navier-Stokes equations, given in integral form for a control volume Ω bounded by the closed contour $\delta\Omega$ as:

$$\frac{d}{dt}\int_{\Omega}\omega dxdy + \oint_{\partial\Omega}(Fdy - Gdx) = 0. \qquad (1)$$

In this equation, x and y are Cartesian coordinates, t represents time, F and G are the fluxes of the dependent variables in the directions x and y respectively. The symbol ω is the solution vector which is composed of density ρ, total energy E, and the x,y momentum terms ρu, ρv. The primitive variables are non-dimensionalized using the free stream values of sound speed a_∞, density ρ_∞, dynamic viscosity μ_∞, chord length c, and heat transfer coefficient k_∞.

The numerical solution of the conservation equations is performed over control volumes composed of an arbitrary number of triangular cells as shown in Figure 1. Each control volume consists of a central node i, and an arbitrary number of neighbour nodes, the location of which defines the boundary of the control volume, shown as a dashed line. Data values are associated with the nodes of the grid, yielding a node-centered scheme with overlapping control volumes. Dependent variables are considered to be cell averages, reducing equation (1) to a discrete form:

$$\frac{d\omega_i}{dt} = -\frac{1}{A_i}\sum_{e=1}^{n}(F\Delta y - G\Delta x)_e\,. \qquad (2)$$

The fluxes F and G are linear interpolations along each edge e. The area of each control volume is denoted as A_i, the number of edges in the control volume boundary is n. The terms Δy and Δx are the lengths of an edge e in the y and x coordinates. The discretized equations are time marched to a steady state through a five-stage Runge-Kutta scheme. Convergence acceleration is achieved through local time stepping, residual smoothing, and the multigrid technique. The effects of turbulence are introduced through the one-equation Spalart-Allmaras eddy viscosity model.

The viscous stress terms appearing in the momentum and energy equations require the calculation of the gradient of the velocity components and the temperature. These terms are approximated as follows:

$$(u_x)_i = \frac{1}{A_i}\int_{\Omega}\frac{\partial u}{\partial x}dxdy = \frac{1}{A_i}\sum_{e=1}^{n}(u\Delta y)_e$$

$$(u_y)_i = \frac{1}{A_i}\int_{\Omega}\frac{\partial u}{\partial y}dxdy = \frac{-1}{A_i}\sum_{e=1}^{n}(u\Delta x)_e\,. \qquad (3)$$

The discretization outlined retains the characteristics of a central differencing scheme in that a spatially oscillating solution can satisfy the discrete conservation relations. As a consequence, an artificial damping term must be added to the total flux to control such oscillations. Following Mavriplis and Jameson [9], the artificial dissipation operator is a combination of undivided Laplacian and biharmonic approximations. Flow field values about control volumes such as that shown in Figure 1 are used to form these approximations and ultimately construct the dissipation operator in the following form:

$$D(\omega_i) = \sum_{j=1}^{n} \left[e^2 (\omega_j - \omega_i) - e^4 (d(\omega_j) - d(\omega_i)) \right] \tag{4}$$

The terms e^2 and e^4 are switches to impose the desired damping intensity for the local flow regime. These switches are formed from the Laplacian approximation on the local pressure field. With the pressure switches averaged between neighbour nodes, the damping operator retains a conservative form.

The Laplacian approximation, $d(\omega_i)$, is constructed through the application of Gauss' theorem, and yields a spatially second-order accurate operator independent of the control volume configuration. In the presence of locally linear solutions in ω, this operator will return a null value in the undivided Laplacian term [10]. The advantage of such a property is to create a lower magnitude damping operator for irregularly shaped grids.

The first derivatives of the operator are computed over each cell in a control volume using equation (3). The approximation to the undivided Laplacian term is then determined from:

$$\begin{aligned} d(\omega_i) &= \oint_{\delta\Omega} \left(\frac{\partial \omega}{\partial x} dy - \frac{\partial \omega}{\partial y} dx \right) \\ &= \phi_i \sum_{e=1}^{n} (\omega_x \Delta y - \omega_y \Delta x)_e . \end{aligned} \tag{5}$$

The summation is computed over each edge forming the control volume boundary. Derivative terms along the control volume boundary are obtained from the cell forming the boundary. In highly stretched regions of a grid, the damping operator can attain excessively large magnitudes. The scaling factor ϕ_i, is added to control the magnitude of the damping term in the presence of these high aspect ratio cells. The components of the scaling factor are solution independent and are therefore computed in a preprocessing procedure. The scaling factor is given by:

$$\phi_i = \left[\sum_{j=1}^{n} \frac{2Area_{j,j+1}}{l_{j,j+1}^2} \right] . \tag{6}$$

Referring to the control volume shown in Figure 1, $l_{j,j+1}$ refers to the length of the edge joining nodes j and $j+1$. The $Area_{j,j+1}$ is the area of the triangular cell that contains the edge $j, j+1$ as its outer edge. The biharmonic operator is created using a differencing stencil similar to that shown in equation (4). This dissipation method has been shown to be effective in obtaining smooth solutions for viscous aerodynamic flows while preserving the conservative nature of the solution [14].

Grids are generated using an advancing front technique combined with Bowyer's algorithm [13] to produce a Delaunay triangulation. Node insertion begins at the airfoil boundary and proceeds outward using local node density to locate sites for possible node placement [15].

Adaptive Gridding Technique

Adaptive gridding uses the solution on a grid of intermediate node density to direct placement of nodes in generating finer grids. The objective is to obtain a grid with superior node placement to one of equal node density generated without knowledge of the solution. The newly generated fine grids are then used with the intermediate parent grid in the multigrid routine.

The adaptation process begins with the calculation of an adaptation parameter (Φ) on the edges of the intermediate mesh after a solution has been obtained. The undivided density and Mach number gradient are computed and normalized with their grid extrema, as follows:

$$\Phi = \frac{|\rho_1 - \rho_2|}{\rho_{max} - \rho_{min}} + \frac{|M_1 - M_2|}{M_{max} - M_{min}} . \tag{7}$$

Locations 1 and 2 are the nodes at each end of a given edge. The selection of density and Mach number as adaptation parameters offers sensitivity to flow discontinuities, stagnation points, and boundary layers. New nodes are placed at the midpoint of edges that have the highest adaptation parameter. Boundary edges are selected and adapted based on the curvature criterion developed by Mavriplis [12]. The adaptation of a grid is performed in two passes, causing regions of high gradients to be heavily adapted. The two pass method can subdivide a large triangle into 16 smaller ones.

After the new points have been introduced into the grid, edge placement is altered in a post-processing retriangulation process. Grids formed of nearly equilateral triangular elements offer reduced truncation error in inviscid regions. The Delaunay triangulation criterion is frequently used to construct grids with this equiangular property. A grid achieves the Delaunay criterion when the sum of the minimum internal angles of all triangles is maximized. Edges are swapped over the entire grid in an iterative process until the criterion is achieved. In regions dominated by viscous effects, adaptive node placement and the Delaunay retriangulation can lead to undesirable grid characteristics. Adaptive gridding can add nodes to regions with stretched cells, and subsequent Delaunay retriangulation will destroy the stretched nature of the local grid, as shown in Figure 2. To prevent such undesirable retriangulations, the grid can be locally stretched in the direction of the prevailing gradient before the Delaunay algorithm is implemented. The resulting retriangulation will not destroy the high aspect ratio nature of any local grid. In fact, this method is solution dependent, conforming to the character of the local flow field. Initially the gradient of the Mach number is computed and averaged over the four nodes of a pair of triangles that share a common edge (M_x, M_y). A stretching parameter S is then formed and used to temporarily place the four nodes into their stretched locations before the Delaunay criterion is locally enforced. It is given by:

$$S = \left[\frac{(M_x \Delta x + M_y \Delta y) + \varepsilon}{|M_x \Delta x + M_y \Delta y + \varepsilon|} l^2 C \right] \tag{8}$$

$$X_i^1 = X_i^o + \frac{M_x}{M_\infty} S \tag{9}$$

$$Y_i^1 = Y_i^o + \frac{M_y}{M_\infty} S \tag{10}$$

The lengths Δx and Δy are the distances from the midpoint of the edge to the neighbour nodes of the quadrilateral under consideration. Here the superscript '1' refers to the location in the stretched space and 'o' refers to the original location. The parameter l is the edge length and C is a stretching coefficient, set to a value of 2.0. The term ε is a very small number used to prevent singularities.

Figures 3 and 4 demonstrate the effect of the solution-dependent retriangulation. An adapted grid with unstretched Delaunay retriangulation is shown in Figure 3. The triangulation procedure sporadically creates nearly equilateral cells in the boundary layer regions. This will result in inflated truncation error and poor solution resolution. With the stretched Delaunay retriangulation shown in Figure 4, the adapted grid retains the locally stretched nature desired in the boundary layer.

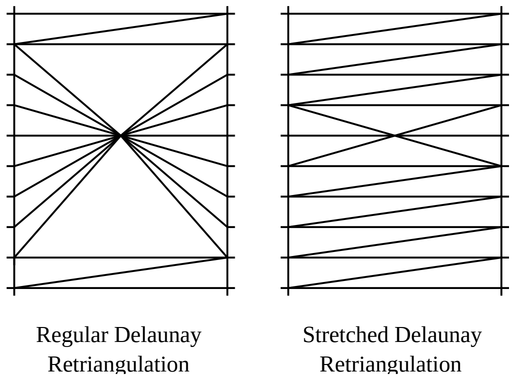

Figure 2: Comparison of regular and stretched Delaunay retriangulation for a new node introduced into a high aspect ratio region

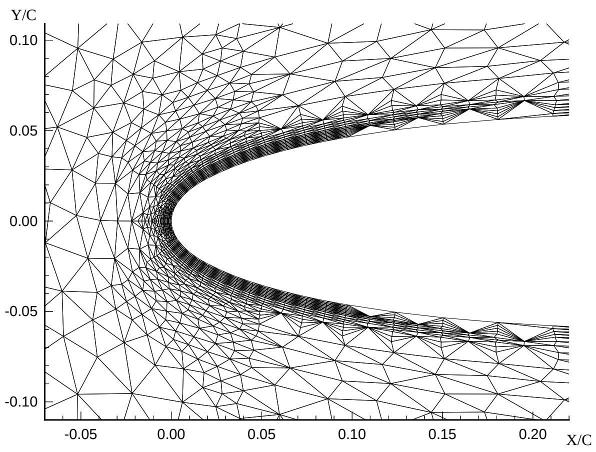

Figure 3: Adapted grid, unaltered retriangulation

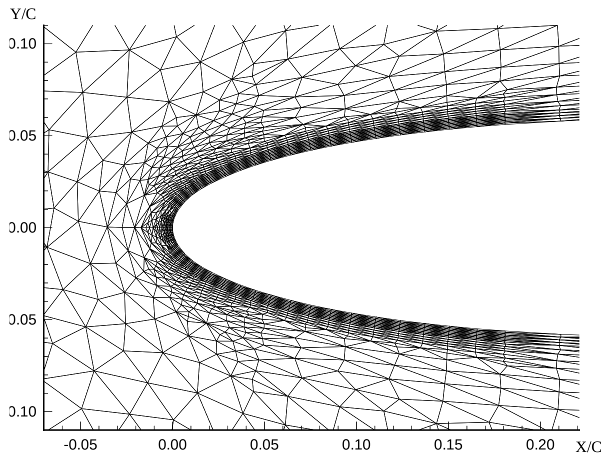

Figure 4: Adapted grid, stretched retriangulation

Results and Discussion

Three cases are studied to assess the solution improvement resulting from the adaptive gridding algorithm. All cases use the NACA 0012 airfoil. The first case has a free stream Mach number of 0.5 with a Reynolds number of 5,000 at 0.0 degrees angle of attack. The second case has a free stream Mach number 0.8 with a Reynolds number of 500 and 10.0 degrees angle of attack. For the third case, the freestream Mach number is 0.16, with an angle of attack of 6.0 degrees and a Reynolds number of 2.88 million. At this Reynolds number the flow is turbulent. Transition is at 0.05 chords on the upper surface and 0.80 chords on the lower.

For the first case, five grids with progressively greater nodal density are used without adaptation. Table 1 shows the total number of nodes in each grid, the number of nodes on the airfoil body, and the initial off-wall spacing at the body surface. The results of the finest grid are considered to be grid independent, and are used as a benchmark result for error calculations. Table 2 provides the total drag and friction drag values along with the error when compared to the benchmark solution.

The test case was recomputed using adapted grids, yielding the results shown in table 3. The first entry was achieved by adaptation of the 736 node grid shown in Table 1. The adapted grid contained 2,944 nodes after the adaptation process. The results show an improvement in total drag over those shown in Table 2 for grid 2 which has roughly the same number of nodes. The total drag error is reduced by 56%. Comparing the second adapted grid, which was obtained from grid 2, the error reduction is approximately 60% when compared to the unadapted grid 3, which has a comperable number of nodes. Figure 5 graphically demonstrates this error reduction over the unadapted results. Here, N is the number of nodes in each grid.

Table 1: Grid characteristics for case 1

Grid	Total nodes	Nodes on body	Off-wall spacing
1	736	36	0.0008
2	2,733	72	0.0004
3	9,682	144	0.0002
4	38,541	288	0.0001
5	50,400	580	0.00005

Table 2: Unadapted Results

Grid	C_d	C_{d_f}	%error C_d
1	0.0699	0.0334	24.3
2	0.0577	0.0336	2.7
3	0.0565	0.0335	0.5
4	0.0560	0.0330	0.3
5	0.0562	0.0331	0.0

Table 3: Adapted results

Nodes	C_d	C_{d_f}	%error C_d
2944	0.0569	0.0335	1.2
10932	0.0563	0.0331	0.2

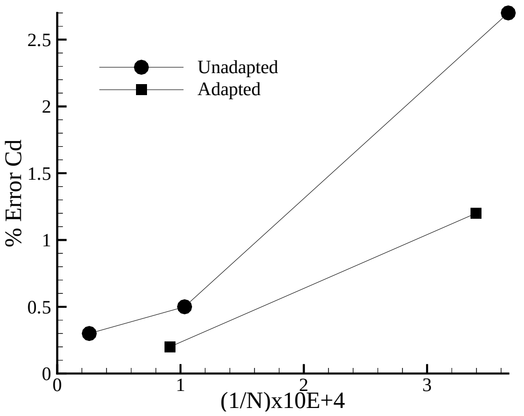

Figure 5: Comparison of unadapted and adapted error in total drag coefficient

Table 4: Grid characteristics for case 2

Grid	Total nodes	Nodes on body	Off-wall spacing
1	780	60	0.0125
2	2,665	120	0.00625
3	9,754	240	0.003125
4	38,767	480	0.00150
5	90,418	800	0.00080

For the second test case, results were obtained using a set of five grids with the characteristics given in Table 4. The finest grid is again used as a reference for error estimation. The lift coefficient for this grid is 0.448, with a pressure drag coefficient of 0.276 and frictional drag coefficient of 0.127. The adapted grids were generated from the first three grids of the set. Figures 6, 7 and 8 show the lift, pressure drag, and friction drag coefficients for both

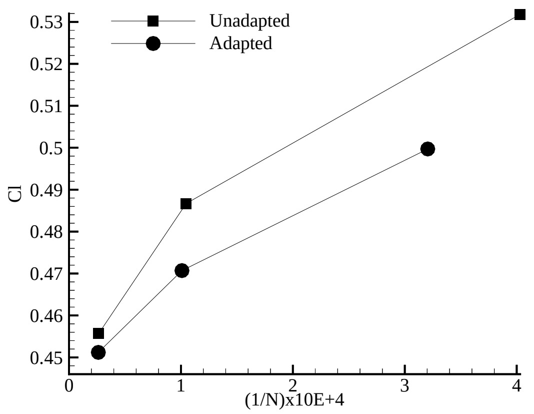

Figure 6: Adapted and unadapted lift coefficient

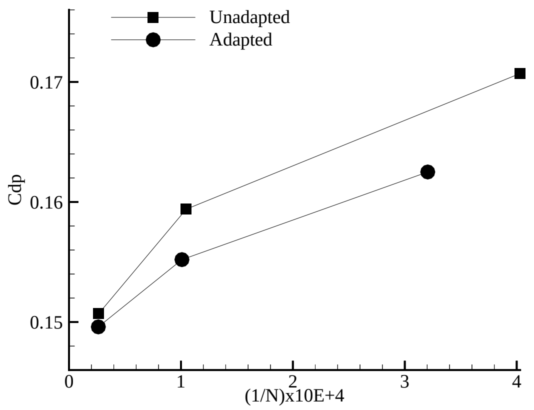

Figure 7: Adapted and unadapted pressure drag coefficient

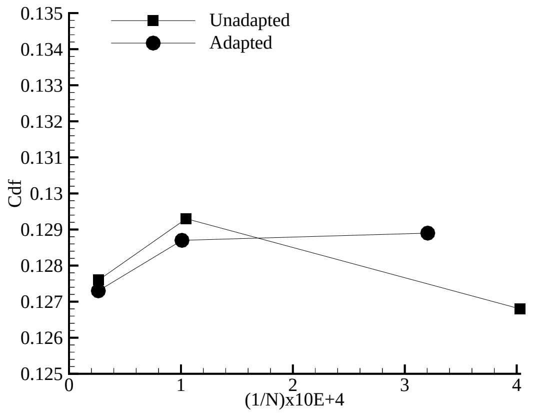

Figure 8: Adapted and unadapted friction drag coefficient

adapted and unadapted grids. In general, results for the adapted grids show a significant reduction in error. Figures 9 and 10 show grid 3 and the adapted grid with 9,500 nodes. Table 5 shows the adapted and unadapted error when compared to the grid independent solution. The results indicate that as the node density increases, the adaptive gridding becomes more effective. For example, at 3,100 nodes the reduction in error of the lift coefficient achieved with the adapted grid is approximately 40%, while at 38,000 nodes the reduction in error is of the order of 60%. Modification of the initial grid characteristics does not alter these conclusions.

Table 5: Percent error between the results of unadapted and adapted grids

Grid nodes	C_l unadapt.	C_l adapt.	C_{d_p} unadapt.	C_{d_p} adapt.
~3,000	18.5	11.4	14.1	8.7
~9,500	8.4	4.9	6.7	4.0
~38,000	1.5	0.6	1.1	0.0

The objective of the final test case is to assess the performance of the adaptive gridding scheme in a more demanding environment. In the previous test cases, adequate resolution of the boundary layer regions and surface shear stresses was achieved through modest off-wall spacing and cell aspect ratio. In this test case, the high Reynolds number necessitates a much higher cell aspect ratio and closer attention to off-wall spacing.

Following the first test case, a series of grids with progressive refinement is again used to assess the performance of the adaptive gridding scheme. Table 6 provides details of the grids used in this test case. Roughly grid independent results were obtained on a grid of approximately 74,000 nodes with 1,200 nodes on the airfoil body and an initial off-wall spacing of 1×10^{-6}. The lift coefficient for this grid was found to be 0.6620, the pressure drag coefficient 0.003230 and the friction drag coefficient 0.003639.

Table 6: Grid characteristics for case 3

Grid	Total nodes	Nodes on body	Off-wall spacing
1	1,450	120	0.00015
2	3,415	180	0.00010
3	5,768	240	0.00005
4	13,751	360	0.000032
5	22,062	480	0.000015

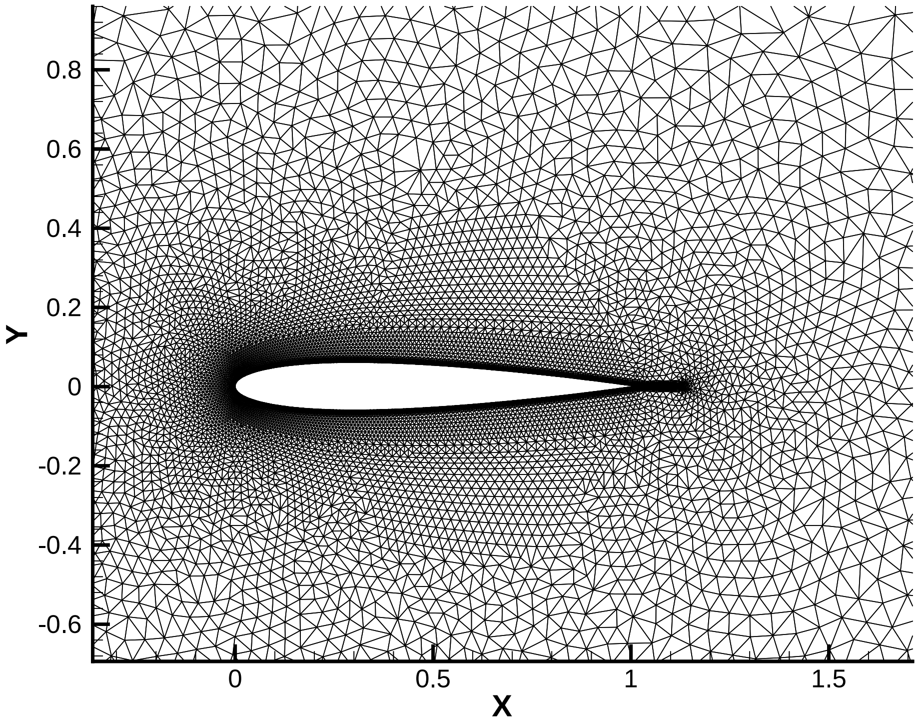

Figure 9: Unadapted grid 3

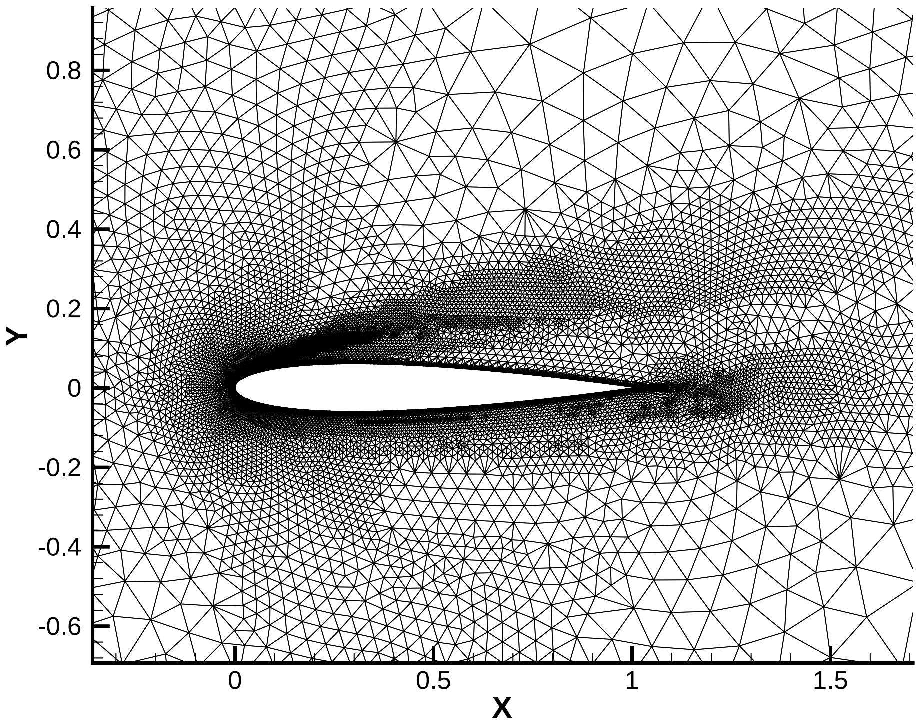

Figure 10: Adapted grid with 9,500 nodes

Table 7: Unadapted grid errors

Grid	% C_l	% C_{d_p}	% C_{d_f}
3	7.31	165.8	69.0
4	6.72	91.7	63.2
5	4.68	40.0	48.8

Table 8: Adapted grid error
Adaptation parameter: density, Mach no.

Equivalent Grid	% C_l	% C_{d_p}	% C_{d_f}	strategy
3	6.34	61.7	77.3	55/45
3	5.13	60.8	77.7	70/30
4	0.00	50.7	75.9	55/45
4	3.02	50.7	76.6	70/30
5	0.16	24.0	63.0	55/45
5	1.58	25.8	65.1	70/30

Table 9: Adapted grid error
Adaptation parameter: pressure, Mach no.

Equivalent Grid	% C_l	% C_{d_p}	% C_{d_f}	strategy
3	6.84	52.5	77.3	55/45
3	4.53	58.7	78.4	70/30
4	1.01	50.2	76.1	55/45
4	3.08	50.0	77.1	70/30
5	0.47	25.4	64.4	55/45
5	1.87	26.3	66.3	70/30

Solutions were computed on grids 1, 2 and 3, then adapted twice to produce grids with node densities similar to grids 3, 4 and 5 respectively. The complete adaptation increases the node density of each grid by approximately a factor of 4. The number of nodes added in each of the two adaptations can be varied to place emphasis either on the viscous regions or the inviscid areas near the airfoil. To this end, two adaptation strategies were selected; the first places 70% of the new nodes in the first adaptation and 30% in the second, while the second configuration places 55% in the first and 45% in the second. The adaptation parameter can also change the emphasis of the adaptation scheme. In the previous test cases the adaptation parameter was based on density and Mach number differences only. However, in this case not only is the density and Mach number parameter used, but an adaptation parameter based on pressure and Mach number differences is also investigated.

The test case was computed on the unadapted grids and the percent error of the results relative to the grid independent solution are shown in Table 7. The lift coefficients for the unadapted grids are compared to adapted results with grids of equivalent node density in Figure 11. Figures 12 and 13 show the pressure drag and friction drag comparisons. Adaptation was based on density and Mach number. Generally, the adapted grids yield a better prediction of the grid independent results than the unadapted grids. The adapted lift and drag coefficients shown in Figures 11 and 12 clearly show a significant improvement. The discrepancy between these values and the grid independent ones are presented as error measures in Tables 7 and 8. The difference in the two adaptation strategies is very small with regard to predictions of drag, but more prominent when considering lift. The 55%/45% strategy is generally superior. With this approach, at least 50% reductions in lift error and 45% reductions in pressure drag error are achieved on grids 4 and 5.

When the adaptation parameter is based on pressure and Mach number differences, the results shown in Table 9 and Figure 14 are obtained. Results are quite similar, with the 55%/45% strategy again preferred.

The surface pressures for grid 4 using the adapted and unadapted methods were compared to those predicted by a well-known algorithm for structured grids. A grid of 40,000 nodes with 300 on the airfoil body and 100 in the off-wall direction with an initial off-wall spacing of 1×10^{-7} was used with the NASA Ames algorithm ARC2D [16]. A comparison of the surface pressures for the unadapted case is shown in Figure 15. Figure 16 shows a corresponding plot for the adapted grid obtained using the 55%/45% strategy, with the equivalent number of nodes as grid 4. The adapted surface pressure more closely follows the structured grid results near the suction peak at the leading edge and on the lower surface near the trailing edge.

In contrast to the results for lift and pressure drag, the present adaptation procedure does not improve the prediction of skin friction drag, which is strongly dependent on the off-wall spacing and the artificial dissipation model. This demonstrates that a grid which is optimal for one parameter may be non-optimal for another.

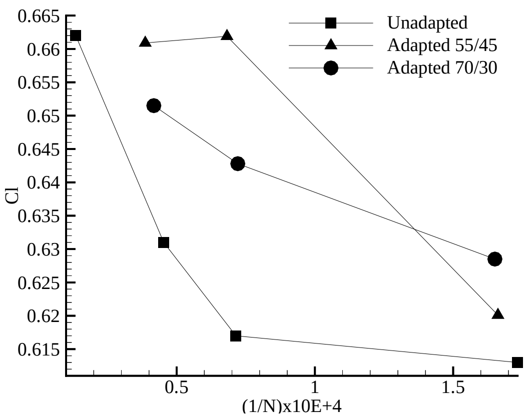

Figure 11: Comparison of lift coefficients for adapted and unadapted grids

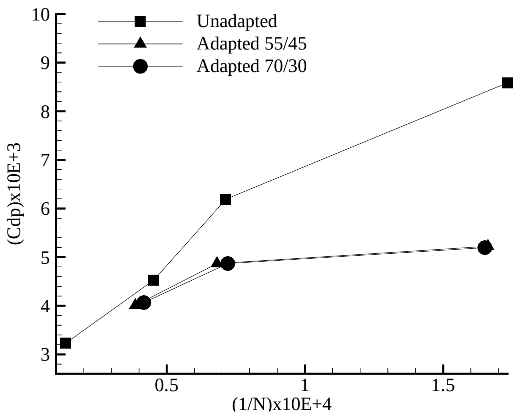

Figure 12: Comparison of pressure drag coefficients for adapted and unadapted grids

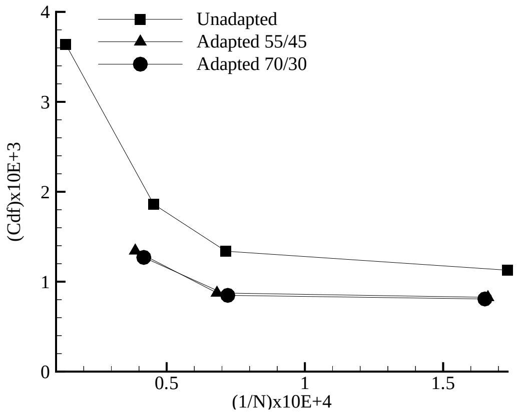

Figure 13: Comparison of friction drag coefficients for adapted and unadapted grids

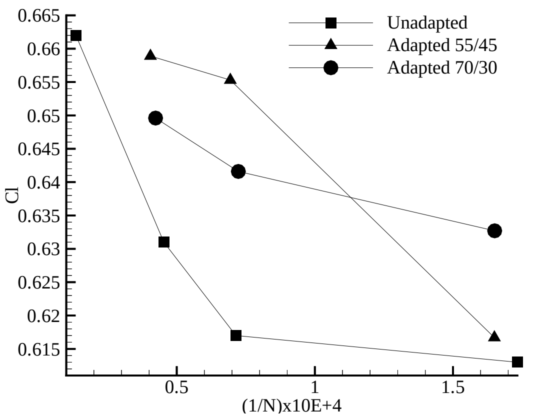

Figure 14: Comparison of lift coefficients for adapted and unadapted grids using pressure/Mach no. for adaptation

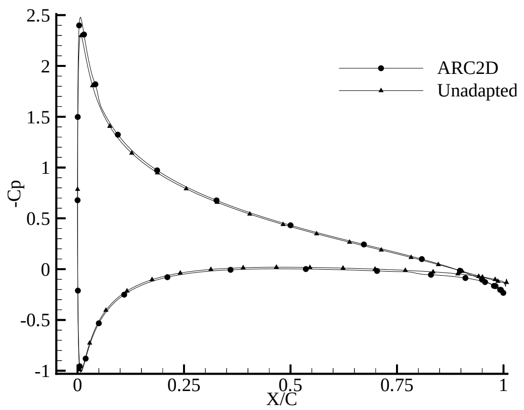

Figure 15: Comparison of surface pressure for the unadapted grid 4 and ARC2D

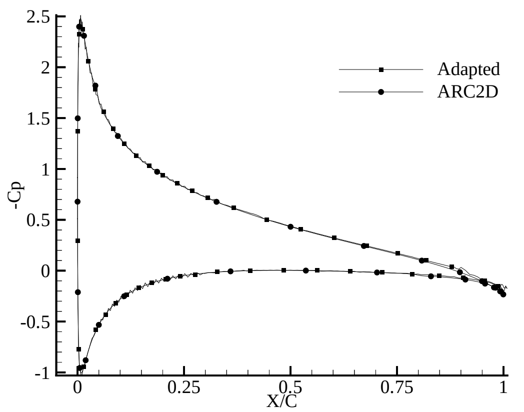

Figure 16: Comparison of surface pressure for the adapted grid and ARC2D, using the density/Mach no. adaptation parameter

Conclusions

This paper has presented a quantitative study of the error reduction achieved with a solution-adaptive gridding algorithm. The results show that a 30-50% reduction in lift and drag coefficient error over unadapted results is possible for aerodynamic flows. Such studies can be used to further improve the adaptation strategy. In particular, the present approach is unsuccessful in improving skin friction drag estimates in high Reynolds number flows. An increase in the number of adaptation passes may be required if this is a critical parameter. Future work will concentrate on multi-element airfoil flows.

References

[1] Zingg, D.W., "Grid Studies for Thin-Layer Navier-Stokes Computations of Airfoil Flowfields", AIAA J., Vol. 30, No. 10, pp. 2561-2564, 1992.

[2] South, J.C., Jr., Thomas, J.L., and Van Rosendale, J., eds., "ICASE /LaRC Workshop on Adaptive Gridding Methods", NASA CP 3316 Oct. 1995.

[3] Powell, K.G., "The Adaptive Cut-Cell Cartesian Approach (Warts and All)", ICASE/LaRC Workshop on Adaptive Gridding Methods, South, J.C., Jr., Thomas, J.L., and Van Rosendale, J., eds., NASA CP 3316, Oct. 1995.

[4] Mavriplis, D.J., "Multigrid Solution Strategies for Adaptive Meshing Problems", ICASE/LaRC Workshop on Adaptive Gridding Methods, South, J.C., Jr., Thomas, J.L., and Van Rosendale, J., eds., NASA CP 3316, Oct. 1995.

[5] Ingram, C.L., Laflin, K.R., and McRae, D.S., "A Structured Multi-Block Solution-Adaptive Mesh Algorithm With Mesh Quality Assessment", ICASE/LaRC Workshop on Adaptive Gridding Methods, South, J.C., Jr., Thomas, J.L., and Van Rosendale, J., eds., NASA CP 3316, Oct. 1995.

[6] Hall, D.J., and Zingg, D.W., "Viscous Airfoil Computations Using Adaptive Grid Redistribution", AIAA J., Vol. 33, No. 7, pp. 1205-1210, July 1995.

[7] Mavriplis, D.J., and Venkatakrishnan, V., "A Unified Multigrid Solver for the Navier-Stokes Equations on Mixed Element Meshes", AIAA paper 95-1666, June 1995.

[8] Warren, G., Anderson, W.K., Thomas, J., and Krist, S., "Grid Convergence for Adaptive Methods", AIAA paper 91-1592, June 1991.

[9] Mavriplis, D.J., Jameson, A., "Multigrid Solution of the Navier-Stokes Equations on Triangular Meshes", AIAA J., Vol. 28, No. 8, pp. 1415-1425, Aug. 1990.

[10] Lindquist, D.R. "A Comparison of Numerical Schemes on Triangular and Quadrilateral Meshes", M.Sc.A.A. thesis, M.I.T., May 1988.

[11] Jameson, A., Mavriplis, D., "Finite Volume Solution of the Two-Dimensional Euler Equations on a Regular Triangular Mesh", AIAA 85-0435, Jan. 1985.

[12] Mavriplis, D., "Unstructured and Adaptive Mesh Generation for High Reynolds Number Viscous Flows", NASA ICASE 187534, Feb. 1991.

[13] Barth, T.J., "Aspects of Unstructured Grids and Finite Volume Solvers for the Euler and Navier-Stokes Equations", von Karman Institute, Brussels, Belgium, March 1994.

[14] Walsh, P., Zingg, D.W., "A Solution- Adaptive Solver for Aerodynamic Applications Using Unstructured Grids", Proceedings of the 4th CFD Society of Canada conference, Ottawa, Canada, June 1996.

[15] Predovic, D.T., "Multigrid Solution of the Euler Equations Using Unstructured Adaptive Meshes", Univ. of Toronto, M.A.Sc. thesis, April 1994.

[16] Pulliam, T.H., "Efficient Solution Methods for the Navier-Stokes Equations", Lecture notes for the Von Karman Institute for Fluid Dynamics Lecture Series: Numerical Techniques for Viscous Flow Computation in Turbomachinery Bladings, Brussels, Belgium, Jan. 20-24 1986.